# Raman, FTIR and theoretical evidence for dynamic structural rearrangements of vanadia/titania DeNOx catalysts

Nan-Yu Topsøe [a,*], Mark Anstrom [b] and J.A. Dumesic [b]

[a] *Haldor Topsøe Research Laboratories, Nymøllevej 55, Lyngby, Denmark*
[b] *Department of Chemical Engineering, University of Wisconsin, Madison, WI 53706, USA*

Received 6 April 2001; accepted 19 June 2001

Insight into the selective catalytic reduction (SCR) of NO by $NH_3$ over vanadia/titania catalysts is obtained from a combination of Raman and FTIR spectroscopic investigations and density functional theory (DFT) calculations. Studies of the V–OH and V=O functional groups under different conditions coupled with calculations of the stability and mobility of H atoms provide evidence that dynamic structural rearrangements may occur during the SCR reaction. Hydrogen atoms are bonded more strongly to oxygen atoms that are coordinated to a single vanadium atom (V=O species), compared to bonding at oxygen atoms that are coordinated to multiple vanadium atoms (*e.g.*, V–O–V species); and, activation energy barriers for hydrogen transfer from a V=O species to another V=O species and to a V–O–V species are estimated from DFT calculations to be 60 and 130 kJ/mol, respectively. This dynamic nature of hydrogen transfer between oxygen atoms having different coordination environments also appears to explain some of the spectroscopic changes observed for vanadia/titania catalysts having different vanadia loadings.

**KEY WORDS:** FTIR; Raman; DFT; dynamic structural rearrangement; vanadia/titania catalyst; SCR-DeNOx

## 1. Introduction

The removal of $NO_x$ in flue gas emitted from power plants remains a major environmental issue today. Despite significant developments in alternative types of $NO_x$ removal processes and catalysts, the most widely used process today is the selective catalytic reduction (SCR) by ammonia over vanadia–titania based catalyst. Over the years, fundamental investigations [1–16] have been carried out to understand the structural aspects of the catalyst, the nature of the active sites and the reaction mechanism. For example, Inomata *et al.* [1] proposed that surface V=O sites are related to the catalytic activity, while Janssen *et al.* [2,3] extended the active structure to be O=V–O–V=O moieties. Later, Went *et al.* [4,5] found that both monomeric and polymeric vanadyl species were involved in the SCR reaction; however, the former species led to higher selectivity in $N_2$. Several other studies [6–16] have proposed V–OH species as being the likely active sites. Our previous studies [12–16] have provided evidence that both V–OH and V=O groups are required for the SCR reaction. The reaction may be initiated by adsorption of ammonia on V–OH species, followed by an activation of the adsorbed ammonia by interaction with V=O. The activated ammonia may then react with gaseous or weakly adsorbed nitric oxide to yield nitrogen and water [14–16]. The various different views from experiments regarding the mechanistic aspects of the SCR reaction have recently motivated several theoretical studies on the vanadium oxide system [17–22].

Despite discrepancies about the detailed nature of the system, there is general consensus from experimental studies that the reaction involves V–OH groups or V=O species or both functionalities. In the literature it has been reported that the temperature and the presence of water have significant effects on the selectivity [23]. Thus, in order to understand the origin of these effects and to probe further the mechanism of the SCR reaction, the present Raman and FTIR spectroscopic investigation was conducted to address the nature of these V–OH and V=O functional groups and their dependence on temperature and water. To help interpret the experimental observations, theoretical calculations using density functional theory (DFT) were performed on various vanadium oxide clusters.

## 2. Experimental

The catalysts studied were 0.6, 2 and 6 wt% $V_2O_5/TiO_2$. These samples were prepared by impregnating the titania support (from Bayer, anatase form, surface area of 90 $m^2/g$) with an oxalic acid solution of ammonium metavanadate, followed by drying at 375 K and calcination at 675 K for 1 h.

Infrared spectra were recorded on a Bio-Rad FTS575C FTIR spectrometer with an MCT (mercury–cadmium telluride) detector at a spectral resolution of 4 $cm^{-1}$. The samples were studied as self-supporting wafers (30 $mg/cm^2$) in an *in situ* cell with $CaF_2$ windows. All IR spectra are shown after baseline correction.

The laser Raman spectra were measured on a Dilor Labram laser Raman system equipped with a confocal microscope. The excitation source used for the present meas-

* To whom correspondence should be addressed.

1011-372X/01/0900-0011$19.50/0 

urements is a 632.8 nm HeNe laser, which delivered about 8 mW power at the sample. The *in situ* cell used is a Linkam THMS 600 thermal stage. The catalysts are studied as pressed pellets. All Raman spectra are shown after baseline correction.

## 3. DFT calculation methods

Quantum chemical calculations employing density functional theory were conducted to probe the energetics for various types of vanadium oxide clusters and to probe the bonding of hydrogen atoms on different types of oxygen atoms in these clusters. The clusters used in this study were constructed from the crystal structure of $V_2O_5$ [24] by selecting adjacent vanadium atoms and all oxygen atoms bonded directly to these vanadium cations. Hydrogen atoms were added to maintain charge neutrality.

The DFT calculations were carried out using DEC workstations with the Jaguar software package (Schrodinger, Inc.) The chosen DFT method uses a hybrid method employing Becke's three-parameters approach, B3LYP [25]. This functional combines the exact HF exchange, Slater's local exchange functional, Becke's 1988 non-local gradient correction to the exchange functional, with the correlation functionals of Vosko–Wilk–Nusair (VWN) and Lee–Yang–Parr (LYP).

The basis set employed in all calculations (LACVP**) uses an effective core potential on all V atoms, developed at Los Alamos National Laboratory by Hay and Wadt [26]. The electrons treated explicitly on V are the outermost core and valence electrons ($3s^2 2p^6 4s^2 3d^3$). The H, N, and O atoms have been treated with the 6-31G** basis set, with all electrons being treated explicitly.

The energy change for hydrogen addition to each cluster was determined for the following stoichiometric reaction:

$$\mathrm{H(g)} + \mathrm{V}_x\mathrm{O}_y\mathrm{H}_z \text{ cluster} \rightarrow \mathrm{V}_x\mathrm{O}_y\mathrm{H}_{z+1} \text{ cluster}$$

Accordingly, we calculate the energy change of this reaction, $\Delta E_{\mathrm{H}}$, from the following terms:

$$\Delta E_{\mathrm{H}} = (E_{\mathrm{VH}}) - (E_{\mathrm{V}} + E_{\mathrm{H}}),$$

where $E_{\mathrm{H}}$ is the energy of a gaseous H atom, and $E_{\mathrm{V}}$ and $E_{\mathrm{VH}}$ represent the energies of the $\mathrm{V}_x\mathrm{O}_y\mathrm{H}_z$ cluster and the $\mathrm{V}_x\mathrm{O}_y\mathrm{H}_{z+1}$ cluster, respectively.

## 4. Results

### *4.1. In situ Raman studies*

Vanadia/titania catalysts containing 0.6, 2, and 6% vanadia were studied *in situ* under a flow of 14.8% $O_2$/Ar (60 ml/min) as a function of temperature. The Raman spectra obtained for the 6% $V_2O_5/TiO_2$ sample are shown in figure 1. The spectrum in the region from 840 to 1100 $cm^{-1}$ (figure 1(a)) obtained at room temperature prior to the heat

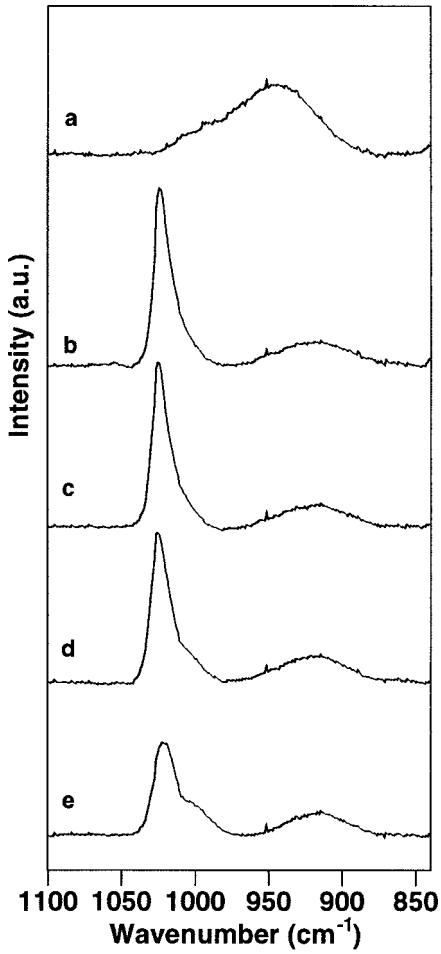


Figure 1. Raman spectra of the 6% $V_2O_5/TiO_2$, (a) at ambient condition, and after heating in a flow of $O_2$/Ar at 673 K for 16 h (b), and subsequently cooled to (c) 573 K, (d) 373 K and (e) room temperature.

treatment shows a broad band feature below 1000 $cm^{-1}$. This spectrum changed significantly upon heat treatment. Figure 1(b) shows the spectrum at 673 K after treatment in flowing $O_2$ at 673 K for 16 h. A well-defined band at 1028 $cm^{-1}$ appears together with a broad band at around 923 $cm^{-1}$. The higher frequency band can be assigned to isolated terminal V=O species [4,27–29], while the broad band feature at lower frequency may be attributed to bridge-bonded V–O–V species in polymeric vanadyl structures [27–29]. Upon cooling in flowing $O_2$ (figure 1 (c)–(e)), the intensity of the high frequency V=O band gradually decreases, whereas the band due to polymeric structures remains unchanged. At room temperature (figure 1(e)), the high frequency band has broadened somewhat and shifted slightly downward with the appearance of a shoulder. It is important to note that these structures appear to represent different equilibrium distributions, since these spectral changes were found to be reversible upon subsequent heating.

Figure 2 compares the spectra at 673 K in flowing $O_2$ of the 6% $V_2O_5/TiO_2$ sample with those of the 0.6 and 2% $V_2O_5/TiO_2$ catalysts. It is seen that the high frequency terminal V=O band is present in all three samples, but the band

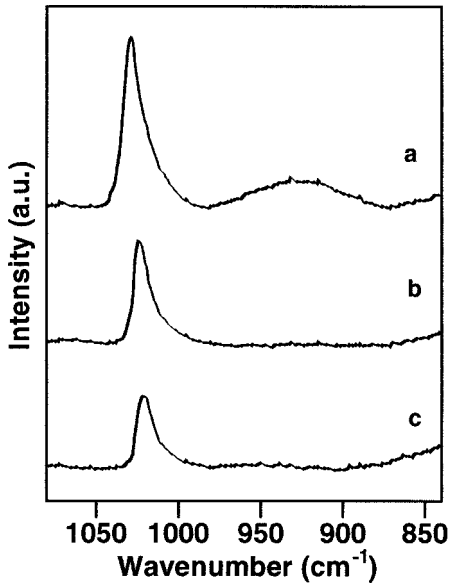


Figure 2. Raman spectra of (a) 6% $V_2O_5/TiO_2$, (b) 2% $V_2O_5/TiO_2$, and (c) 0.6% $V_2O_5/TiO_2$ at 673 K after pretreatment in a flow of $O_2$/Ar at 673 K for 16 h.

intensity and frequency decrease as the vanadia loading is lowered on the titania surface. Moreover, the broad band feature near 923 $cm^{-1}$ seen in the 6% $V_2O_5/TiO_2$ sample is not present in the spectra of the two samples with lower vanadia loading. The decrease in the intensity of the high frequency terminal V=O band shows that the number of terminal V=O groups decreases for lower vanadia loadings, whereas the simultaneous downward frequency shift reflects a lengthening of the V=O bond. The absence of the broad band feature at lower vanadia loadings indicates that significant amounts of polymeric vanadia species are not present in catalysts with vanadia loadings lower than 2%.

To study how water can affect the surface structure, *in situ* Raman spectra were recorded for the 6% $V_2O_5/TiO_2$ catalyst at various temperatures under a flow of $O_2$ containing saturated water vapor. These spectra are reported in figure 3. Only negligible difference in the V=O band is detected upon changing from flowing $O_2$ to a flow of $O_2$ and $H_2O$ at 673 K (compare figure 3(b) with figure 1(b)). When the temperature is lowered, the intensity of the terminal V=O band decreases slightly, while the intensity of the broad band at lower frequency increases (figure 3 (c) and (d)). At room temperature, larger spectral changes caused by water are observed (figure 3(e)). Besides a large intensity decrease, the high frequency V=O band has broadened and shifted downwards to 1018 $cm^{-1}$. In addition, the intensity of the lower frequency band ($\sim$914 $cm^{-1}$) has increased significantly. Note that this spectrum at room temperature is different from the spectrum of the hydrated sample (figure 3(a)) prior to heat treatment in $O_2$.

### *4.2. In situ FTIR studies*

Figure 4 shows IR spectra in the O–H stretching vibration region of 6% $V_2O_5/TiO_2$ (figure 4(a)), 2% $V_2O_5/TiO_2$

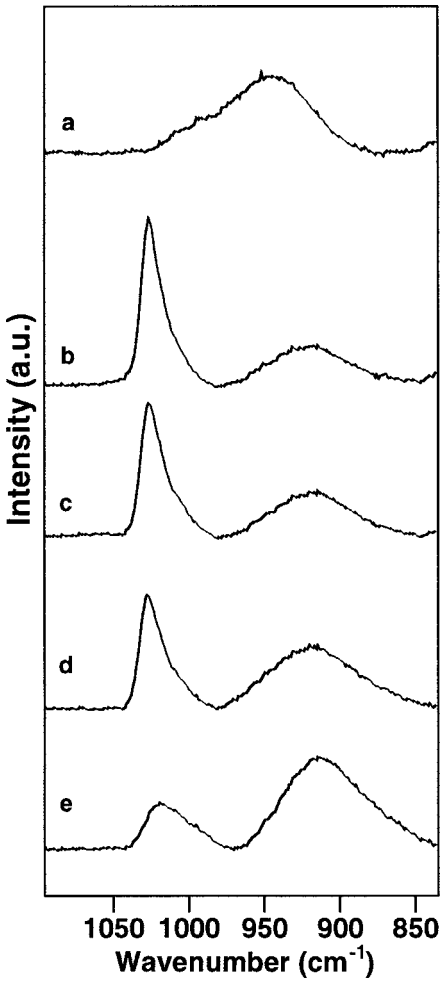


Figure 3. Raman spectra of the 6% $V_2O_5/TiO_2$ (a) at ambient condition, and after heating in a flow of $O_2$/Ar at 673 K for 16 h and subsequently exposed to $O_2$ + $H_2O$/Ar flow at (b) 673 K, (c) 573 K, (d) 373 K, and (e) room temperature.

(figure 4(b)) and the titania support (figure 4(c)) (all wafers are of the same thickness). The characteristic bands at 3720, 3674, and 3645 $cm^{-1}$, which are due to the different hydroxyl groups on the titania surface [30], are replaced by mainly a band at 3667 $cm^{-1}$ for the 2% $V_2O_5/TiO_2$ catalyst. A somewhat weaker broad band envelope at slightly lower frequency is observed for the 6% $V_2O_5/TiO_2$ catalyst. This, according to previous studies [12,14,15,31] is attributed to V–OH groups. Figure 5(a) shows a series of IR spectra in the O–H stretching region of the 6% $V_2O_5/TiO_2$ catalyst under a flow of $O_2$/Ar as a function of temperature. Prior to recording these spectra, the sample had been pretreated in flowing $O_2$ at 673 K for 16 h and cooled to room temperature. The series of spectra show that the band intensity decreases significantly with increasing temperature (from top to bottom). The intensity of the O–H band is considerably higher at room temperature (top spectrum), and the band consists of an overlap of several band contributions. At increasing temperatures, the high frequency band contribution at 3655 $cm^{-1}$ gradually decreases, such that a broad band centered at 3633 $cm^{-1}$ remains at 673 K (bottom spectrum).

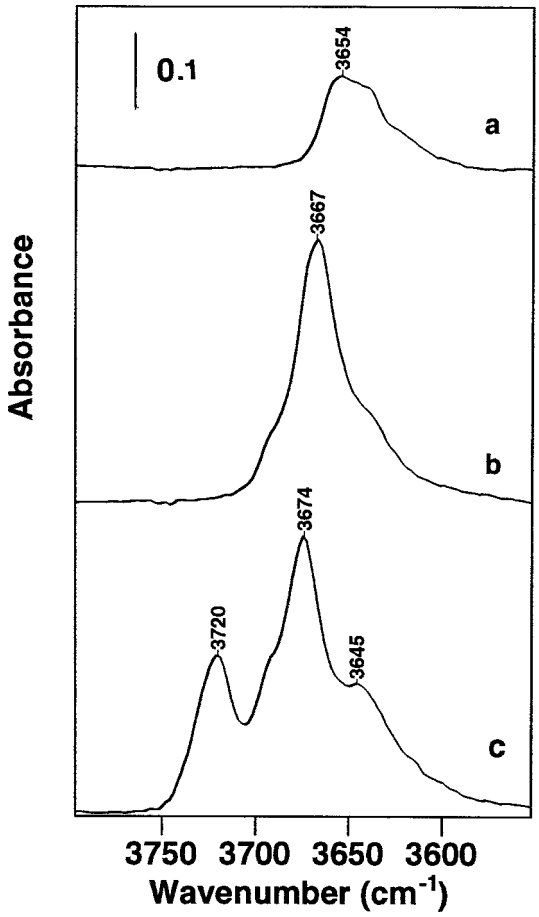


Figure 4. FTIR spectra in the OH stretching regions of (a) 6% $V_2O_5/TiO_2$, (b) 2% $V_2O_5/TiO_2$, and (c) $TiO_2$ (similar thickness used in all samples).

These spectral changes with varying temperatures are completely reversible with temperature, as shown in figure 5(b), where the sample has been cooled to again room temperature.

Figure 5(c) shows the same series of spectra but in the spectral region, 2200–1900 $cm^{-1}$, corresponding to the first overtone vibrational band of V=O species [31]. In contrast to the O–H stretching band region, the V=O band centered at 2036 $cm^{-1}$ is slightly more intense at higher temperatures (top spectrum). At lower temperatures, the band can be resolved into two bands at 2042 and 2004 $cm^{-1}$ (bottom spectrum). As observed for the VO–H band, the spectral feature in the V=O overtone band is completely restored upon cooling to room temperature (figure 5(d)).

Experiments were carried out on the 2% $V_2O_5/TiO_2$ catalyst and the $TiO_2$ support to probe whether the O–H stretching vibration region showed the same variation with temperature as exhibited by the 6% $V_2O_5/TiO_2$ catalyst. Figure 6 shows the IR spectra of these samples in the O–H stretching region recorded at different temperatures. In contrast to the 6% $V_2O_5/TiO_2$ sample, the relative spectral changes are much smaller for the 2% $V_2O_5/TiO_2$ catalyst (figure 6(a)) and even smaller for the titania support (figure 6(b)).

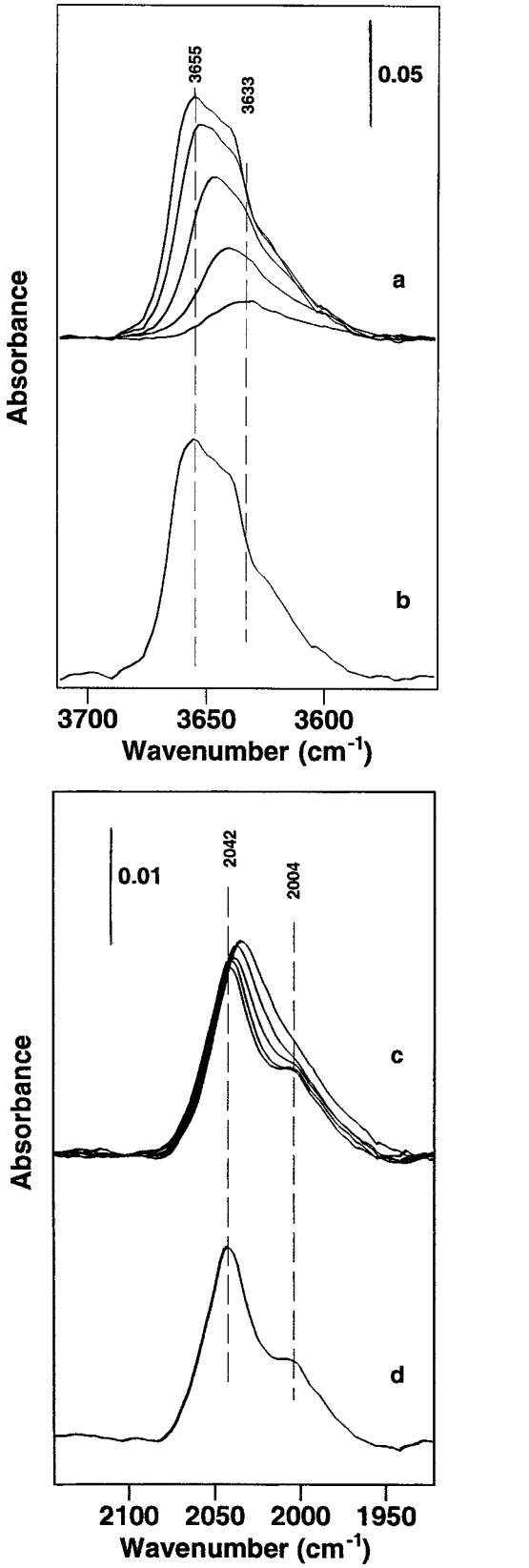


Figure 5. FTIR spectra of the V–OH (a, b), and V=O overtone band (c, d) of the 6% $V_2O_5/TiO_2$ pretreated in a flow of $O_2$/Ar at 673 K for 16 h, and (a, c) cooled to room temperature, and subsequently reheated to 373, 473, 573, and 673 K (from top to bottom), and (b, d) is recorded after cooling to room temperature again.

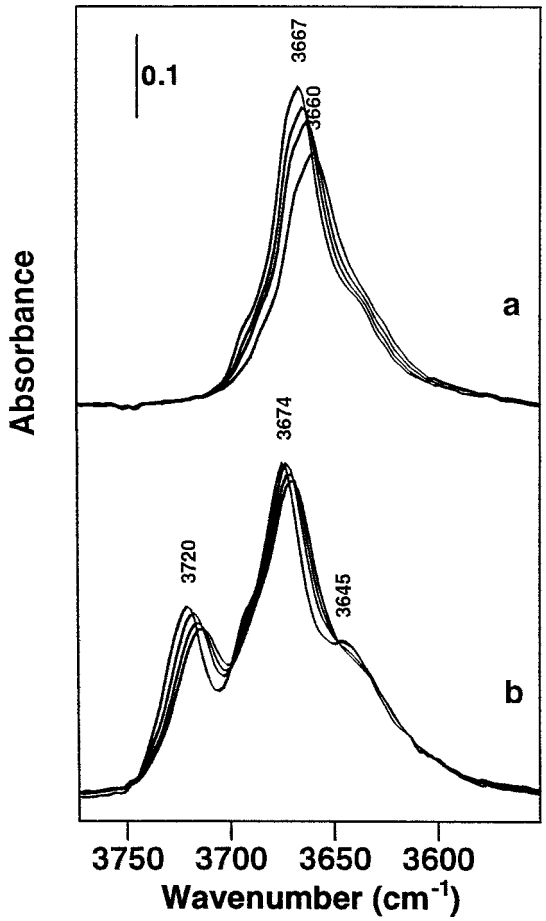


Figure 6. FTIR spectra in the OH stretching region of (a) 2% $V_2O_5/TiO_2$, and (b) $TiO_2$ pretreated in a flow of $O_2$/Ar at 673 K for 16 h and cooled to room temperature, and subsequently reheated to 373, 473, and 573 K (from top to bottom).

### *4.3. DFT calculations*

#### *4.3.1. Energetics for bonding H atoms to $V_xO_yH_z$ clusters*

The crystal structure of $V_2O_5$ [24] contains vanadium atoms that are coordinated to oxygen atoms in a distorted octahedral geometry. Each vanadium atom is capped by a doubly-bonded vanadyl oxygen atom with a bond length of 154 pm, and also shares four single bonds (177–202 pm) with four neighboring oxygen atoms. The octahedral coordination is completed by a weak (281 pm) bond with a vanadyl oxygen atom belonging to the vanadium atom in the crystal layer beneath it. This structure contains oxygen atoms coordinated to 1, 2 or 3 vanadium atoms, denoted as O[1], O[2] or O[3], respectively.

To probe the energetics for the bonding of H atoms to the different oxygen atoms in the vanadia structure, clusters containing 2 and 3 vanadium atoms were constructed. These clusters (denoted as $V_2$ and $V_3$, respectively) are shown in figure 7, and they are based on the following stoichiometries: $V_2O_7H_4{\cdot}(H_2O)_2$ and $V_3O_{11}H_7$. Each cluster was initially constructed by taking the appropriate number of vanadium atoms from a (010) plane of $V_2O_5$, including all oxygen atoms within the plane that are directly bonded to these

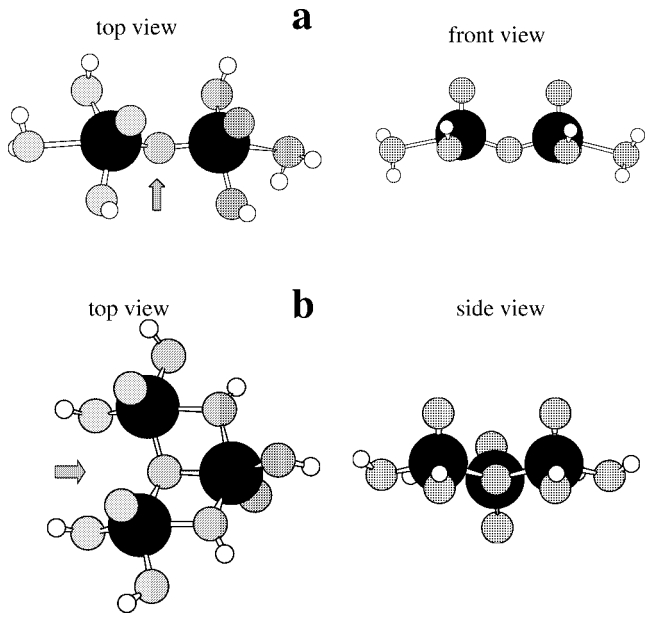


Figure 7. Structures of $V_2$ and $V_3$ clusters. (a) Top and front view of $V_2$ cluster, (b) top and side view of $V_3$ cluster. Arrows indicate direction of view.

vanadium atoms. Hydrogen atoms were then added to each cluster to maintain charge neutrality. As seen in figure 7, these clusters contain terminal hydroxyl groups as well as coordinated water.

The geometries of these vanadium oxide clusters were optimized to minimize the total electronic energy according to three scenarios. In the first scenario, the V=O and V–O bond lengths were optimized, while the positions of the vanadium atoms were fixed, the V–O–H angles were fixed, the V=O groups in the clusters containing 2 or 3 vanadium atoms were constrained to be parallel, and the O=V–O–H dihedral angles were held constant. In the second scenario, the positions of the V atoms were also allowed to relax, while maintaining all other constraints (*i.e.*, the V–O–H angles were fixed, the V=O groups in the clusters containing 2 or 3 vanadium atoms were constrained to be parallel, and the O=V–O–H dihedral angles were held constant). In the third scenario, the V–O–H angles were also optimized to minimize the electronic energy, while maintaining the remaining constraints (*i.e.*, the V=O groups in the clusters containing 2 or 3 vanadium atoms were constrained to be parallel, and the O=V–O–H dihedral angles were held constant). For the $V_2$ cluster, the positions of the hydrogen atoms belonging to the coordinated water molecules were fully relaxed in each of the three optimization scenarios. Values for the different V–O distances in the $V_2O_7H_4{\cdot}(H_2O)_2$ and $V_3O_{11}H_7$ clusters are presented in table 1 for the three geometry optimization scenarios.

Upon optimization of the $V_2O_7H_4{\cdot}(H_2O)_2$ cluster, the length of the V–$OH_2$ bond was approximately 240 pm in scenarios 1 and 2. Moreover, when the cluster was fully optimized according to scenario 3, the V–$OH_2$ bond length increased to 327 pm, effectively placing the two vanadium atoms in tetrahedral environments. The tetrahedral structure

Table 1
V–O distances (pm) in vanadium oxide clusters for different geometry optimization scenarios.

| | Scenario 1 | Scenario 2 | Scenario 3 |
|---|---|---|---|
| *$V_2O_7{\cdot}(H_2O)_2$ cluster* | | | |
| V=O | 157–158 | 158 | 157–158 |
| V–OH | 180–183 | 180–184 | 177–178 |
| V–O–V | 178 | 178 | 178 |
| V–$OH_2$ | 246–248 | 235–238 | 321–327 |
| *$V_3O_{11}H_7$ cluster* | | | |
| V=O | 156–157 | 157 | 157 |
| V–OH | 177–181 | 178–182 | 177–181 |
| V–O[2]–V | 186–205 | 186–212 | 187–212 |
| V–O[3]–V | 192–194 | 190–203 | 190–199 |

Table 2
V–V and O–H distances (pm) in vanadium oxide clusters for different geometry optimization scenarios.

| Cluster | Scenario 1 | Scenario 2 | Scenario 3 |
|---|---|---|---|
| V–V in $V_2$ | 342 | 341 | 335 |
| V–V in $V_2$–H(O[1]) | 342 | 346 | 343 |
| V–V in $V_2$–H(O[2]) | 342 | 365 | 374 |
| O–H in $V_2$–H(O[1]) | 97.5 | 97.4 | 97.5 |
| O–H in $V_2$–H(O[2]) | 98.0 | 97.8 | 97.9 |
| V–V in $V_3$ | 308–356 | 319–347 | 320–351 |
| V–V in $V_3$–H(O[1]) | 308–356 | 320–350 | 322–348 |
| V–V in $V_3$–H(O[3]) | 308–356 | 333–395 | 330–423 |
| O–H in $V_3$–H(O[1]) | 97.2 | 97.0 | 96.8 |
| O–H in $V_3$–H(O[3]) | 97.3 | 97.3 | 97.3 |

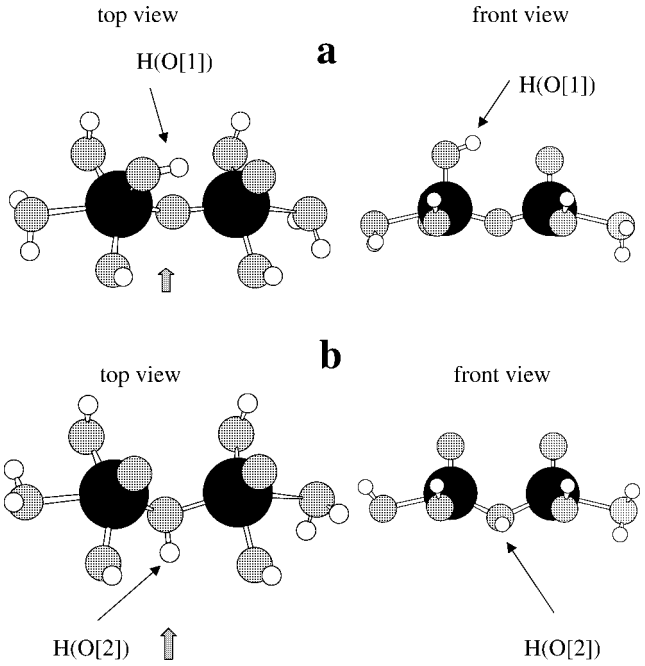


Figure 8. Top and front views of structures of $V_2$ cluster after addition of H atom at (a) the O[1] position and (b) the O[2] position. Arrows indicate direction of view.

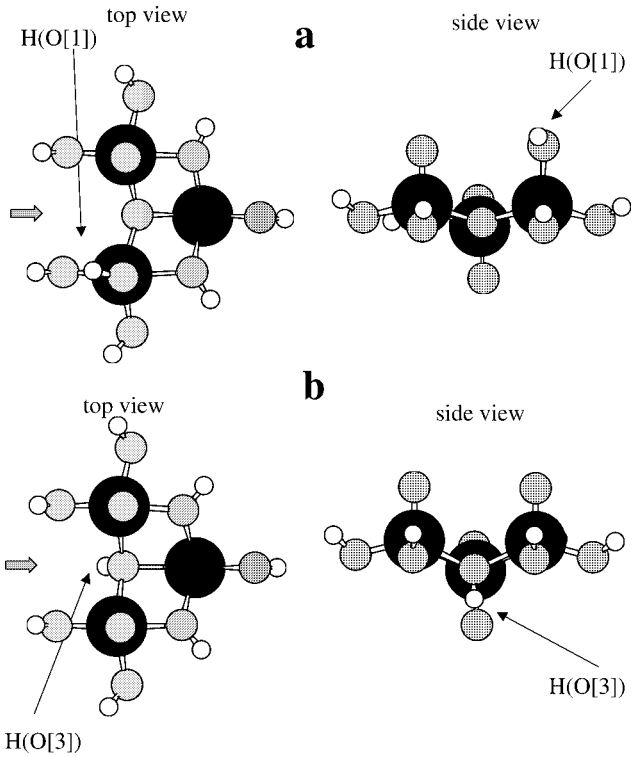


Figure 9. Top and side views of structures of $V_3$ cluster after addition of H atom at (a) the O[1] position and (b) the O[3] position. Arrows indicate direction of view.

observed under full optimization is in agreement with published V-51 NMR [32] and EXAFS [33] results, indicating that the vanadium cations in surface vanadia structures are four-coordinated, with one terminal V=O bond and three bridging V–O bonds. Further details of the bonding of $H_2O$ molecules to vanadium atoms in vanadia clusters will be discussed separately [34].

Figures 8 and 9 show the geometries for the $V_2$ and $V_3$ clusters, respectively, after addition of a H atom to each cluster at the O[1], O[2], and O[3] positions where appropriate. For both the $V_2$ and $V_3$ clusters, it was found that the V–V distances did not change significantly when a hydrogen atom was bound to the cluster at O[1]; however, addition of a hydrogen atom at a bridging oxygen atom (O[2] or O[3]) resulted in significant expansion of the V–V distances. The V–V distances for the $V_2$ and $V_3$ clusters are shown in table 2 for the three geometry optimization scenarios. This table also shows O–H bond lengths for the $V_2$ and $V_3$ clusters after addition of a hydrogen atom at the O[1], O[2], and O[3] positions. It can be seen that the O–H bond is shorter for a hydrogen atom at the O[1] position compared to the O[2] position in the $V_2$ cluster, and the O–H bond is shorter for a hydrogen atom at the O[1] position compared to the O[3] position in the $V_3$ cluster. These trends suggest that the hydrogen atom is bonded more strongly to the O[1] atom in both clusters.

The energy changes for addition of a hydrogen atom to the $V_2$ and $V_3$ clusters are summarized in table 3 for the three geometry optimization scenarios. It can be seen in this table that for each of the geometry optimization scenarios, the energy change for addition of a hydrogen atom at the

Table 3
Energy changes (kJ/mol) for addition of hydrogen atom to $V_2$ and $V_3$ clusters for different geometry optimizationscenarios.

| Reaction | Scenario 1 | Scenario 2 | Scenario 3 |
|---|---|---|---|
| $V_2 + H \rightarrow V_2H(O[1])$ | −298 | −283 | −275 |
| $V_2 + H \rightarrow V_2H(O[2])$ | −199 | −214 | −204 |
| $V_3 + H \rightarrow V_3H(O[1])$ | −265 | −265 | −273 |
| $V_3 + H \rightarrow V_3H(O[3])$ | −201 | −246 | −259 |

Table 4
Vibrational frequencies ($cm^{-1}$) of $V_2$ cluster with a hydrogen atom added at the O[1] and O[2] positions.

| Band | O[1]–H | O[2]–H |
|---|---|---|
| V=O | 1123 | 1070, 1093, 1107, (1091)[a] |
| VO–H | 3708 | 3548 |

[a] DFT intensity-weighted average frequency.

O[1] position for the $V_2$ cluster is more favorable than for addition at the O[2] position. In addition, the energy change for addition of a hydrogen atom at the O[1] position for the $V_3$ cluster is more favorable than for addition at the O[3] position. These results are in agreement with the trends noted above with respect to the O–H bond lengths for the binding of H atoms at the different positions on the $V_2$ and $V_3$ clusters. It is important to note that the energy change for addition of a hydrogen atom at the O[1] position is comparable for the $V_2$ and the $V_3$ clusters. Therefore, the results from DFT calculations on $V_2$ and $V_3$ clusters suggest that the O[1] position is the most favorable site for binding of a hydrogen atom, followed by the O[3] position, and then followed by the O[2] position. Our conclusion that the binding energy for addition of a H atom to an O atom should be stronger at the O[1] position than at the O[2] or O[3] positions is in agreement with DFT calculations for slabs of $V_2O_5$ [22].

*4.3.2. Calculated infrared spectra of $V_2$ clusters*

Vibrational spectra were calculated of the $V_2$ clusters after the addition of a hydrogen atom at O[1] and O[2]. The calculated frequencies of the V=O and VO–H stretching bands for each cluster are shown in table 4. Upon transfer of a hydrogen atom from the O[1] to the O[2] position, the VO–H stretching frequency decreases by 160 $cm^{-1}$ from 3708 to 3548 $cm^{-1}$. Although the calculated magnitude of the frequency shift is greater than the frequency shift observed experimentally, the direction of the shift is consistent with our experimental infrared spectra, in light of our calculations showing that hydrogen addition at O[1] is energetically preferable to hydrogen addition at O[2], and that O[2]–H species should be favored at higher temperatures. The fundamental V=O stretching frequency also shifts slightly (*ca.* 32 $cm^{-1}$) upon transfer of a hydrogen atom from O[1] to O[2], from a value of 1123 $cm^{-1}$ when the hydrogen atom is at the O[1] position to a DFT intensity-weighted average value of 1091 $cm^{-1}$ when the hydrogen atom is at the O[2] position. This downward shift is consistent with the experimental results.

Table 5
Energy changes of reaction ($\Delta E$) and activation energy barriers ($E_{act}$) for hydrogen atom transfer from O[1] to O[1] and from O[1] to O[2].

| Hydrogen transfer | $\Delta E$ (kJ/mol) | $E_{act}$ (kJ/mol) |
|---|---|---|
| O[1] → O[1] | 0 | +60 |
| O[1] → O[2] | +50 | +130 |

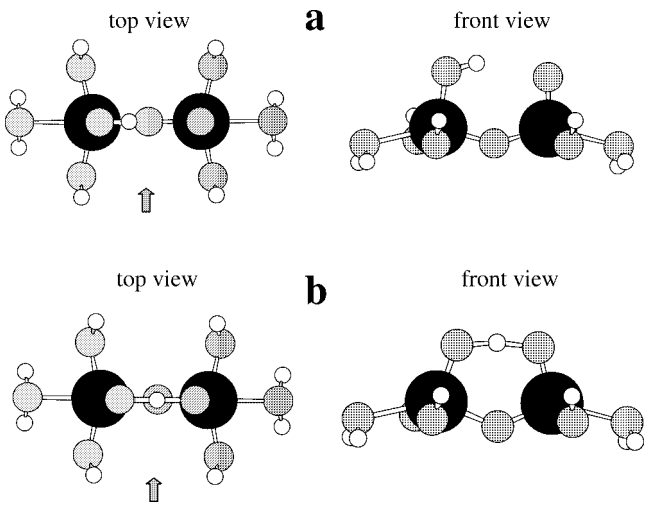


Figure 10. Top and front views of structures of $V_2$ cluster after addition of H atom at O[1] and full relaxation of O[1] atoms: (a) optimized O[1]–H cluster and (b) transition state for hydrogen transfer between O[1] atoms.

*4.3.3. Activation energy barriers for hydrogen transfer*

The activation energy barriers for hydrogen transfer between neighboring O[1] atoms and between O[1] and O[2] atoms were investigated using the $V_2$ cluster. In order to facilitate hydrogen transfer, the $V_2$ cluster was optimized according to scenario 2, but the positions of the O[1] atoms were fully relaxed to allow O=V–V=O bending and twisting. Upon re-optimization of the O[1]–H and O[2]–H clusters, the energy change for transfer of a hydrogen atom from O[1] to O[2] decreased from a value of 69 kJ/mol (see scenario 2 in table 3) to a value of 50 kJ/mol.

The energy changes and activation energy barriers for hydrogen transfer between two O[1] atoms and hydrogen transfer from O[1] to O[2] atoms are listed in table 5. The structure of the re-optimized $V_2$ cluster with the H atom at the O[1] position and the approximate transition state for hydrogen transfer between two O[1] atoms are shown in figure 10. The transfer of a hydrogen atom between neighboring O[1]–H atoms takes place with a modest activation barrier of 60 kJ/mol. The transition state for this hydrogen transfer occurs at a O[1]–H bond distance of 120 pm.

The structure of the re-optimized $V_2$ cluster with the H atom at the O[2] position and the approximate transition state for hydrogen transfer from O[1] to O[2] are shown in figure 11. The transfer of a hydrogen atom from O[1] to O[2] proceeds with an activation barrier of 130 kJ/mol, which is significantly higher than that for hydrogen transfer between two O[1] atoms. The reaction takes place in two steps. The

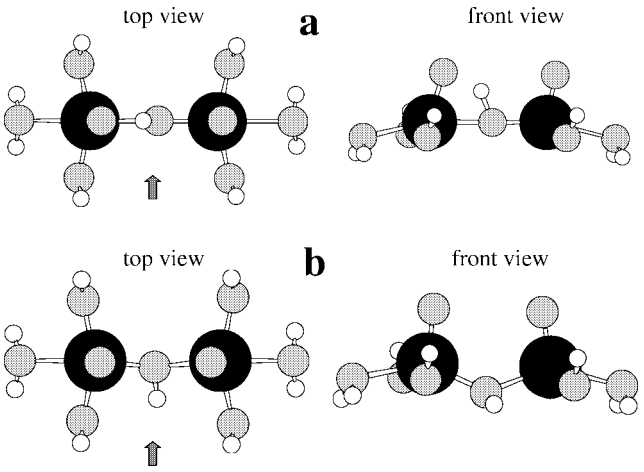


Figure 11. Top and front views of structures of the $V_2$ cluster after addition of H atom at O[2] and full relaxation of O[1] and O[2] atoms: (a) transition state for hydrogen transfer between O[1] and O[2] atoms and (b) optimized O[2]–H cluster.

hydrogen atom at O[1] is first transferred to O[2], passing through an energy maximum at a O[2]–H bond distance of approximately 110 pm. After transfer of the hydrogen atom from O[1] to O[2], the transferred hydrogen atom rotates about the V–V axis until it is pointed away from the two V=O groups. This rotation is a non-activated process.

## 5. Discussion

### *5.1. Dynamic nature of the vanadia surface structures*

Various theoretical studies of vanadia surfaces have been conducted using quantum mechanical calculations based on either cluster [17–21] or periodic slab models [22]. The catalytically important $V_2O_5(010)$ surface contains three structurally different oxygen sites, *i.e.*, oxygen atoms coordinated to one (O[1]), two (O[2]) and three (O[3]) vanadium atoms. It is seen that the results of the present cluster DFT calculations for the binding energies of H atoms on the three different oxygen sites (*i.e.*, O[1]–H > O[3]–H > O[2]–H) are in contrast with previous cluster calculations [17–21] which indicate that the OH bond strength decreases in the order of O[3]–H > O[2]–H > O[1]–H. The discrepancy between our results and previous cluster calculations may be due to the fact that previous cluster studies determined OH bond strength through the addition of a proton, giving the cluster a positive charge, whereas our clusters are electrically neutral. In fact, our results are in agreement with results from previous slab calculations [22].

The present results show that the vanadia structure on the titania surface depends not only on the vanadia loading but also on the temperature. The Raman results show that both monomeric and polymeric vanadia species are present on the catalyst at higher vanadia loading (6%), whereas predominately monomeric vanadia species are present on lower loading catalysts. This behavior is confirmed by the IR results which show that the VO–H band shifts downwards in frequency with increasing vanadia loading, and also that the band intensity decreases significantly with increasing loading. The latter result reflects a relatively lower concentration of hydroxyl groups in the polymeric vanadate structures, which dominate in the higher loading catalysts.

The dynamic nature of the vanadia surface structure is revealed by the temperature dependence of various surface functional groups. The asymmetry of the VO–H band and the presence of an apparent shoulder toward lower frequency for the 6% $V_2O_5/TiO_2$ catalyst suggest the presence of different surface OH groups. The large decrease in the intensity of the VO–H band together with the downward frequency shift in the band position with increasing temperature shown in the IR spectra indicate the presence of surface structural changes. Such temperature effects are apparently smaller for the lower vanadia loading catalyst and minimal for the titania support. Thus, surface structural changes predominate in the high loading catalyst and are thus likely to be associated with the presence of polymeric vanadate species. Further support for this is given below.

A possible interpretation is outlined below for the spectroscopic observations and the theoretical results of the present study. In the lower loading catalyst where mainly monomeric structures are found, the concentration of surface terminal VO–H groups is relatively high in comparison to high loading catalyst where polymeric vanadia structures predominate. At lower temperatures, terminal OH groups are favored, whereas at elevated temperatures, H atoms become mobile, such that some of these atoms are transferred from the energetically favored O[1] position to other positions, including nearby oxygen atoms which are multiply-coordinated to vanadium atoms (*e.g.*, O[2] and O[3] positions). For example, the activation energy barrier calculated in the present study (*i.e.*, 130 kJ/mol) for transfer of a hydrogen atom from O[1] to O[2] leads to a rate constant of *ca.* 1 $min^{-1}$ at 473 K, indicating that this hydrogen transfer is very feasible at the experimental conditions of the present study. The expected increase in O–H bond length caused by the transformation from terminal to multiply-coordinated OH groups is reflected by the observed downward frequency shift with increasing temperature. In addition, the hydrogen atom may also be transferred from the V–O[1] position to form new Ti–OH groups. As a result, the decrease in terminal V–OH is not accompanied by a similar increase in other V–OH bands. Moreover, the band related to the formation of OH groups coordinated to multiple vanadium cations and/or to titanium cations may be rather broad, thereby leading to an apparent decrease in the band intensity. Thus, singly coordinated VO[1]–H groups predominate at room temperature, whereas OH groups coordinated to multiple vanadium cations and/or to titanium cations dominate at higher temperatures.

In contrast to the VO–H band, the overtone band of the V=O groups in the IR spectra does not decrease in intensity with increasing temperature. Rather, a slight increase in intensity is seen at higher temperatures, together with a downward frequency shift. This observation suggests the forma-

tion of new V=O groups with slightly longer bond length. The observation that the opposite trend is seen in the intensity variation as a function of temperature for the V=O overtone band as compared to the VO–H band supports the above scenario regarding the mobility of H atoms at higher temperature, with a simultaneous creation of new terminal V=O groups.

At higher temperatures, hydrogen atoms become mobile on the vanadia/titania catalysts, and they populate the energetically less-favorable bridging oxygen positions, as illustrated:

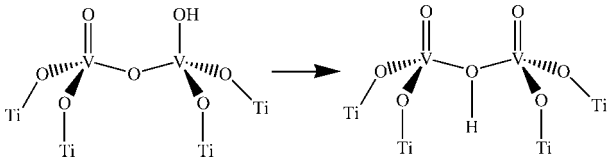

and/or

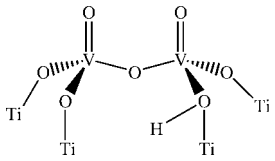

The formation of these structures leads to a decrease in the intensity of the terminal OH band and a shift to lower frequency due to bridged VO–H species, as well as an increase in the number of V=O groups. In contrast, mobility of hydrogen does not occur in the lower loading catalysts where predominately monomeric vanadia structures are present, and the hydrogen atoms appear to be primarily associated with the titania support.

It is interesting that these dynamic changes should result in a temperature dependence for the number of active sites involved in the catalyst, and this behavior may influence the apparent activation energy. It is noteworthy that such dynamic effects would be expected to dominate in the catalyst with higher vanadia loading, as observed in the present studies. In the above context, it could be recalled that the apparent activation energies of high and low loading catalysts have been reported to be different [35]. Clearly different adsorption characteristics of high and low loading catalysts also play a role [35], but it would be interesting to reinterpret the kinetics also taking into account the present dynamic changes in the concentration of active sites.

### *5.2. Influence of water on surface structures*

The Raman spectra of the 6% $V_2O_5/TiO_2$ catalyst (figure 1) show that after dehydration at higher temperature, water is removed from the surface such that terminal V=O and polymeric V–O–V structures are formed. The observed decrease in the intensity of the terminal V=O band and the appearance of a shoulder towards lower frequency at lower temperatures are consistent with the above proposal of dynamic structural changes with temperature. It is however apparent that the extent of the mobility of H atoms can also depend on the degree of dehydration, since our Raman results show that much larger intensity variations are observed for samples subjected to less extensive dehydration pretreatment. As vanadia/titania catalysts are never completely dehydrated under realistic SCR reaction conditions, such dynamic effects may well play an important role in the reaction.

On the extensively dehydrated vanadia surface, there is little influence of water on the surface vanadyl structures at temperatures above 573 K. However, at lower temperatures, as also seen previously by Amiridis *et al.* [36], the effect of water on the surface structure is mainly reflected in the Raman spectra by some broadening in the terminal V=O band and enhancement in the intensity of the polymeric V–O–V band. The spectral changes seen in the V=O band indicate some coordination with water *via* hydrogen bonding. The increase in the band intensity of the polymeric V–O–V is most likely related to an increasing degree of polymerization associated with extensive solvation of surface vanadia species.

## 6. Conclusions

Significant changes are observed in the surface V–OH and vanadyl structures with varying temperatures. In accordance with results from DFT calculations on vanadium oxide clusters, these changes observed in the *in situ* IR and Raman spectra can be explained by the mobility of H atoms at elevated temperatures. Specifically, this dynamic phenomenon involves a temperature dependent transfer of H atoms from the singly coordinated terminal VO[1]–H groups to multiply coordinated oxygen atoms, accompanied by the formation of new terminal V=O groups. DFT calculations show that hydrogen atoms are bonded more strongly to oxygen atoms that are coordinated to a single vanadium atom (V=O species), compared to bonding at oxygen atoms that are coordinated to multiple vanadium atoms (*e.g.*, V–O–V species). The activation energy barriers for hydrogen transfer from an O[1] atom to another O[1] atom and to an O[2] atom are 60 and 130 kJ/mol, respectively. The dynamic structural rearrangement is found not only to depend on the temperature but also on the vanadia loading and water. The mechanistic implications of these findings on the SCR reaction are presently being investigated.

## Acknowledgement

Stimulating discussions with Dr. Henrik Topsøe are gratefully acknowledged. We also wish to acknowledge funding from Basic Energy Sciences at the Department of Energy for funding work conducted at the University of Wisconsin.

## References

[1] M. Inomata, A. Miyamoto and Y. Murakami, J. Catal. 62 (1980) 140.
[2] F. Janssen, F. van den Kerkhof, H. Bosch and J. Ross, J. Phys. Chem. 91 (1987) 5921.

[3] F. Janssen, F. van den Kerkhof, H. Bosch and J. Ross, J. Phys. Chem. 91 (1987) 6633.
[4] G.T. Went, L.-J. Leu and A.T. Bell, J. Catal. 134 (1992) 479.
[5] G.T. Went, L.-J. Leu, R. Rosin and A.T. Bell, J. Catal. 134 (1992) 492.
[6] M. Takagi, T. Kawai, M. Soma, T. Onishi and K. Tamaru, J. Catal. 50 (1977) 441.
[7] R.A. Rajadhyaksha and H. Knözinger, Appl. Catal. 51 (1989) 81.
[8] J.P. Chen and R.T. Yang, J. Catal. 125 (1990) 411.
[9] U. Ozkan, Y. Cai and M. Kumthekar, J. Catal. 149 (1994) 390.
[10] M. Gasior, J. Haber, T. Machej and T. Czeppe, J. Mol. Catal. 43 (1988) 359.
[11] H. Schneider, S. Tschudin, M. Schneider, A. Wokaun and A. Baiker, J. Catal. 147 (1994) 5.
[12] N.Y. Topsøe, J. Catal. 128 (1991) 499.
[13] N.Y. Topsøe and H. Topsøe, Catal. Today 9 (1991) 77.
[14] N.Y. Topsøe, H. Topsøe and J. Dumesic, J. Catal. 151 (1995) 226.
[15] N.Y. Topsøe, J. Dumesic and H. Topsøe, J. Catal. 151 (1995) 241.
[16] J. Dumesic, N.Y. Topsøe, H. Topsøe, Y. Chen and T. Slabiak, J. Catal. 163 (1996) 409.
[17] K. Hermann, A. Michalak and M. Witko, Catal. Today 32 (1996) 321.
[18] A. Michalak, M. Witko and K. Hermann, Surf. Sci. 375 (1997) 385.
[19] M. Witko, R. Tokarz and J. Haber, Appl. Catal. A 157 (1997) 23.
[20] M. Witko, K. Hermann and R. Tokarz, Catal. Today 50 (1999) 553.
[21] K. Hermann, M. Witko and R. Druzinic, Faraday Discuss. 114 (1999) 53.
[22] X. Yin, H. Han, I. Gunji, A. Endou, M. Kubo, K. Teraishi, A. Chatterjee and A. Miyamoto, J. Phys. Chem. B 103 (1999) 1263.
[23] N.Y. Topsøe, T. Slabiak, B. Clausen, T. Srnak and J. Dumesic, J. Catal. 134 (1992) 742.
[24] A. Byström, K. Wilhelmi and O. Brotzen, Acta Chim. Scand. 4 (1950) 1119.
[25] D. Becke, J. Chem. Phys. 98 (1993) 5648.
[26] J. Hay and W.R. Wadt, J. Chem. Phys. 82 (1985) 299.
[27] M.A. Vuurman, I.E. Wachs and A.M. Hirt, J. Phys. Chem. 95 (1991) 9928.
[28] I.E. Wachs, G. Deo, B.M. Weckhuysen, A. Andreini, M.A. Vuurman, M. de Boer and M.D. Amiridis, J. Catal. 161 (1996) 211.
[29] J.-M. Jehng, G. Deo, B.M. Weckhuysen and I.E. Wachs, J. Mol. Catal. A 10 (1996) 41.
[30] G. Busca and L. Marchetti, J. Chem. Soc. Faraday Trans. I 81 (1985) 1003.
[31] G. Busca, Langmuir 2 (1986) 577.
[32] H. Eckert and I.E. Wachs, J. Phys. Chem. 93 (1989) 6796.
[33] M. Ruitenbeek, A.J. Van Dillen, F.M.F. de Groot, I.E. Wachs, J.W. Geus and D.C. Konigsberger, Topics Catal. 10 (2000) 241.
[34] M. Anstrom, J.A. Dumesic and N.Y. Topsøe, in preparation.
[35] T.Z. Srnak, J. Dumesic, B.S. Clausen, E. Törnqvist and N.Y. Topsøe, J. Catal. 135 (1992) 246.
[36] M.D. Amiridis, I.E. Wachs, G. Deo, J.M. Jehng and D.S. Kim, J. Catal. 161 (1996) 211.